Biophysical Journal
Article

Biophysical Society

Sliding Mechanism at a Coiled-Coil Interface

David Gomez,[1] Yulian Gavrilov,[1] and Yaakov Levy[1,*]
[1]Department of Structural Biology, Weizmann Institute of Science, Rehovot, Israel

ABSTRACT The α-helical coiled coil (CC) is a common protein motif that because of the simplicity of its sequence/structure relationship, it has been studied extensively to address fundamental questions in protein science as well as to develop strategies for designing protein with novel architectures. Nevertheless, a complete understanding of CC structures and their dynamics is still far from achieved. Particularly, spontaneous sliding at interfaces of CC proteins was observed for some systems, but its mechanism and usage as an intrinsic conformational change at CCs in protein-protein interfaces is unclear. Using coarse-grained and atomistic simulations, we study various sequences of homodimeric CC, in both parallel and antiparallel configurations. Both the strength of the hydrophobic core and the existence of salt bridges at the periphery of the interface affect sliding dynamics at the CC interface. Although the energy landscape for sliding along a CC interface is different for parallel and antiparallel configurations, both are characterized by a free energy of 1–1.5 kcal/mol, depending on the residues that constitute the CC interface. These barrier heights suggest that sliding kinetics is relatively slow in CC systems and are not expected to be of long length scale, yet they can be involved in functional motions. Our study explains the sliding that has been experimentally observed for the antiparallel CC of the dynein stalk region and the nuclear pore complex and suggests that this one-dimensional motion is an intrinsic feature in CC systems that can be involved in other CC systems.

INTRODUCTION

Biomolecular dynamics and plasticity, which are essential to many biomolecular processes, span large length- and timescales. These processes range from fast local fluctuations to slow extensive structural rearrangements. Their conformational dynamics and transition are spatially complex and nontrivial to predict. A particular, relatively simpler case of biomolecular dynamics is manifested in one-dimensional (1D) diffusion in which two biomolecules slide relative to each other along a main axis. During sliding, the biomolecules interact more weakly (i.e., with lower affinity) compared with the high-affinity complex formed when they interact specifically. Intermolecular sliding dynamics mediates important cellular functions and was reported for several biomolecular systems.

It is well established that sliding dynamics is involved in the facilitated diffusion of a protein searching for its target site on double-stranded DNA (dsDNA). Various features of protein sliding along DNA were studied extensively using a variety of experimental, theoretical, and computational approaches (1–3). Other proteins were reported to perform sliding dynamics along single-stranded DNA (ssDNA) (4,5). Although universal biophysical principles are probably shared by these sliding processes, the details of their mechanism are highly likely to differ for proteins searching for dsDNA versus ssDNA, both because of the very different natures of the DNA environments and in keeping with the functions of the protein. Sliding dynamics may also take place at protein-protein interfaces. It was reported that some proteins can diffuse along a microtubule, with such sliding mediated by electrostatic interactions, similarly to the diffusion of proteins along DNA (6,7). Sliding was also reported at different protein-protein interfaces, where it occurred between the helices that comprise a coiled-coil (CC) oligomer.

Linear diffusion along protein-protein interfaces can be affected by the ruggedness of the energy landscape on which the sliding takes place. The formation of tight interactions that must be broken to permit sliding constitutes a barrier to it. For example, hydrogen bonds or stronger electrostatic interactions may slow down diffusion. Diffusion of proteins along DNA was shown to be affected by electrostatic interactions (3,4). For many proteins, the energetic ruggedness for sliding along dsDNA is small (~1 kBT) (1,2); however,

Submitted December 17, 2018, and accepted for publication February 26, 2019.

*Correspondence: koby.levy@weizmann.ac.il

David Gomez's present address is School of Mechanical Engineering, Tel Aviv University, Tel Aviv, Israel

Editor: Margaret Cheung.

https://doi.org/10.1016/j.bpj.2019.02.026

© 2019 Biophysical Society.

for several proteins, a greater ruggedness of ~2 kBT was reported (8). The sliding of proteins along dsDNA and ssDNA is allowed when the periodic interface with the DNA is characterized by an underlying energy landscape that is not too rugged. The energy landscape for sliding along dsDNA is expected to be smoother than for ssDNA because its greater rigidity acts as a geometric track for sliding (3). In both cases, the existence of long-range electrostatic interactions may assist the diffusion. Sliding dynamics, however, might be more complex and may involve several diffusion modes (9–12).

The CC is a protein motif that comprises two or more α-helices that wrap around each other and can be found in ~5% of all the proteins (13–15). CCs widely mediate protein-protein interactions and form rigid structures that are often involved in generating forces or in sensing forces in cells (16–18). The biological functions of CCs critically depend upon their affinity, specificity, and the dynamics of helix pairing (19,20). Helices in CCs have a characteristic seven amino acid repeat unit $(abcdefg)_n$, and their functional folding and assembly generally require them to pair hydrophobic residues in the *a* and *d* positions in the dimerization interface and other residues near the interface, as shown in Fig. 1. Because of the relative simplicity of their sequence/structure relationship and their programmable oligomerization recognition, CCs have been studied extensively in folding studies and as models for protein engineering and design (21–23). This is often achieved by mutating positions *a*, *d*, *e*, and *g*, because these residues can regulate the structure (e.g., oligomerization state) and stability of the CC (24–26).

The periodic α-helical structure of CCs and the relative simplicity of their interface can lead to alternative conformations. For example, it was shown that some sequences of dimeric CC can satisfy both parallel (P) and antiparallel (AP) configurations; therefore, a switching transition was observed (27–29). Another conformational plasticity exhibited by CCs is a helix shift, which occurs when the registry of one helix shifts through translation relative to the other, with the length of the translation often one heptad repeat (30–32). Despite their high stability and tight hydrophobic core, sliding motions and staggered conformations have been reported for some CC systems (30,32–34).

It is likely that this intermolecular sliding is related to the periodicity and the quasilinearity of the interface between the helices that comprise the CC. Although the resultant staggered helical structures were first proposed when the high-resolution crystal structure of the CC GCN4 leucine zipper domain was obtained (35), these alternative conformations have only been observed in a few CCs with special sequence patterns that deviate from the canonical heptad repeat. Such helix sliding has important biological functions, especially for relaying conformational changes to distal domains or across membranes. One prominent example is the AP, two-stranded CC contained in the stalk domain of dynein, which connects its ATPase domain and its microtubule-binding domain (MTBD) (31,36).

The kinetics of helix staggering and sliding has not been well characterized, and its molecular mechanisms are unclear. Moreover, it is not known if helix sliding is limited to specific sequences or if it is a general property intrinsic to CCs. A further understanding of these alternative

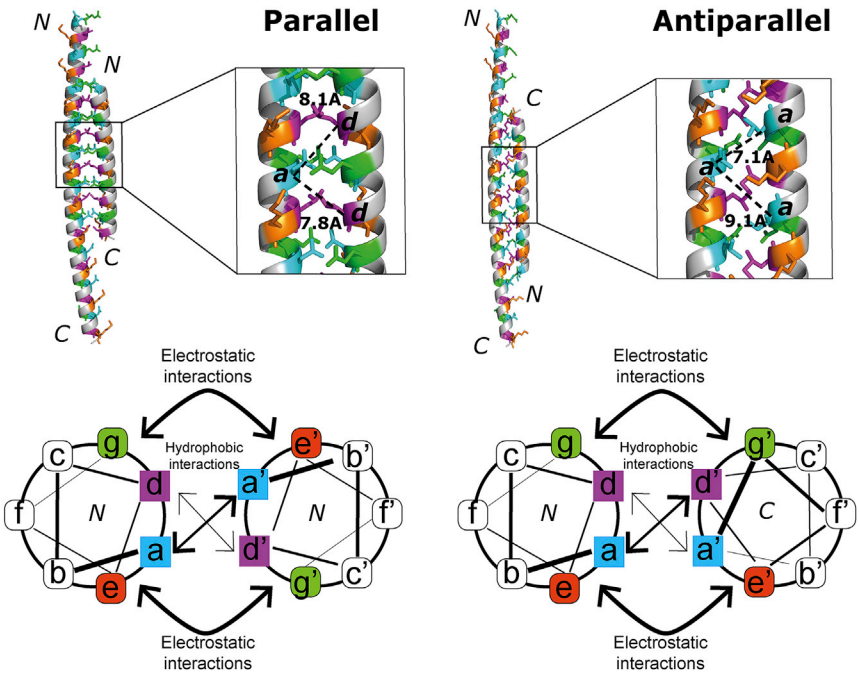

FIGURE 1 Structures of homodimeric coiled-coils (CCs). Model systems of homodimeric P and AP CC configurations. CCs consist of seven amino acids organized in heptad repeats, $(abcdefg)_n$, with *a* and *d* residues forming the CC hydrophobic core and *e* and *g* residues, which are generally charged, interacting in the following ways: g_n:e_{n+1} and *e*-*e'* for P and AP CCs, respectively. P structures are generally more symmetric than AP CCs, with residues equidistantly organized among the heptad repeats. To see this figure in color, go online.

structures and their mechanisms of formation is needed for a better understanding of CC functions and dysfunctions. The difficulty in finding these different conformations is associated with their limited stability. The sliding dynamics in CC might be observed for unique sequences that reduce the stability of the major binding mode and support the shift in registry. Alternatively, one may argue that sliding is an intrinsic dynamics in CCs because of its distinctive periodic structure. These observations led us to explore the mechanisms for CC sliding. In particular, we sought to establish whether sliding is a general property of CCs that arises from the periodicity of their interfaces or whether it is sequence dependent and to identify the energetic contributions to heptad shifting dynamics. A fundamental question to be addressed is the trade-off between the interface stability and sliding speed.

To characterize the mechanisms of CC sliding, we used coarse-grained models and atomistic molecular dynamics (MD) simulations. Specifically, we created different CC systems with different electrostatic charge distributions in the *e* and *g* positions and different hydrophobic residues in the *a* and *d* positions of the heptad repeat unit. We observed that different electrostatic charge patterns lead to different sliding dynamics that is linked to the degree of electrostatic frustration (37) at the interface between the helices. Additionally, we performed umbrella sampling studies in full-atom representations of our models to quantify free energy during the sliding process. Our findings suggest that sliding is an intrinsic dynamic in CC systems that can be modulated by the strength of electrostatic and hydrophobic interactions.

METHODS

The sliding of homodimeric CC was studied using coarse-grained and atomistic simulations.

Coarse-grained models

In the coarse-grained models, each residue is represented by two beads at the Cα and Cβ atoms. Charged amino acids (K, R, H, D, and E) have their charge at the Cβ position. To avoid a decrease in the size of the interface between the helices during sliding of the CC, the helices of the homodimeric CC are of different length. The approach allows the shorter helix (a five-heptad repeat) to slide along a longer helix (a 10-heptad repeat) while maintaining the size of the interface. Each helix of the CC is simulated by a native topology-based model and uses the Lennard-Jones potential to represent native helical contact interactions (38). The electrostatic interactions are modeled by the Debye-Hückel model (39).

We simulated sliding in both P and AP CC configurations by allowing all residues in the *a* and *d* positions from different helices to interact with the unique geometry of each configuration (see Fig. 1). The P CC was modeled by allowing all residues in the *a* and *d* positions from different helices to interact with a distance of 8 Å. The AP CC was modeled by allowing each pair of residues in *a* positions (or in *d* positions) from different helices to interact with a characteristic distance of 7 Å. Because of the asymmetry in the distances between residues in the *a* positions of the AP helices (see Fig. 1), only distances of 7 Å were included to avoid geometrical conflict. To modulate the strength of the interface of the homodimeric CC, we changed the energetic strength of the contacts that constitute the hydrophobic core (i.e., contacts between residues at positions *a* and *d* from different helices) by modifying their Lennard-Jones strength, ϵ. Unless stated otherwise, we set $\epsilon = 1$.

We constructed P and AP homodimer CC models using the web server CCBuilder.01 (40). Sequences were designed by following the well-defined interaction patterns between the *e* and *g* positions for the P and AP conformations (i.e., *g*-e^{+1} and *g*-*e*, respectively), see Fig. 1. In total, six CC models were created: three P and three AP. The P models differ in their electrostatic frustration patterns, described in subscript numbers: $P_{0\rightarrow 0}$, $P_{0\rightarrow 100}$ and $P_{100\rightarrow 100}$. In $P_{0\rightarrow 0}$, all *g*-*e* electrostatic interactions are attractive before and after sliding over one heptad repeat, namely, the CC lacks any electrostatic frustration. In $P_{0\rightarrow 100}$, all the *g*-*e* electrostatic interactions are attractive in the CC initial state but become repulsive after sliding of one heptad repeat, thus increasing its electrostatic frustration. In $P_{100\rightarrow 0}$, all *g*-*e* interactions are all repulsive in the initial state and become attractive after sliding of one heptad repeat. The AP models were built as follows: $AP_{100\rightarrow 100}$ has repulsive electrostatic interactions between all *g*-*e* positions before and after sliding of one heptad repeat. In $AP_{50\rightarrow 50}$, a combination of repulsive and attractive interactions take place between *g* and *e* positions before and after sliding. We note that because of symmetric and geometrical limitations, it is not possible to construct a homodimeric $AP_{0\rightarrow 0}$ model. All simulations were run for a total number of 4×10^8 steps. Every 1000 steps, a snapshot of the CC configuration was taken, such that an ensemble of 4×10^4 configurations was obtained from each simulation.

All-atom models

For unbiased all-atom MD simulations and umbrella sampling, we performed MD simulations for models of both P and AP CC conformations using GROMACS version 2016.3. We used the CCBuilder.01 server to generate 20 models that capture a complete sliding of a single heptad. We conducted an umbrella sampling analysis by running 50-ns MD simulations in an NPT ensemble, for the 20 different structures of each studied CC, in such a way that the energy landscape of a whole sliding event over a heptad repeat was recovered. The force field parameters for the box with the CC protein, SPC water molecules and ions, were derived from the AMBER99SB-ILDN force field. We note that the chosen reaction coordinate follows the helical geometry of the CC and is directly obtained when shifting the helices with respect to each other. The atomistic simulations were performed for several sequences of P and AP CCs that differ with respect to the identity of the residues located in the *a*, *d*, *e*, and *g* positions. For P CC, we studied the following systems: $P_{0\rightarrow 0}$ (*N*-*L*), $P_{0\rightarrow 100}$ (*N*-*L*), $P_{0\rightarrow 0}$ (*L*-*L*), $P_{100\rightarrow 0}$ (*N*-*L*), and $P_{No\ charge}$ (*L*-*L*). The letters in the parentheses refer to the residues in the *a* and *d* positions. For example, in $P_{0\rightarrow 0}$ (N-L), there is an Asn and Leu in the *a* and *d* positions, respectively. The identity of the residues in the other positions follows the notification of the CC systems that were studied using coarse-grained models. The uncharged P and AP sequences were designed by mutating the charged residues (E and K) with S. The CCs were then built using the CCBuilder. Umbrella sampling was also applied to study the sliding process in Nup58/45. More details of the studies CC and their sequence are in the Supporting Materials and Methods.

Table S1 summarizes the sequences studied in the coarse-grained simulations and in the atomistic simulations. Fig. S1 shows these sequences pictorially and highlights the pairing of potential salt bridges between the *e* and *g* sites.

RESULTS

Sliding at the interface of CC proteins may, in principle, be supported by both its periodic nature and its relatively simple geometrical features. Following the importance of

electrostatic interactions for protein sliding along nucleic acids (3,4), we examined their role in the sliding of CC by tuning the number of salt bridges. The effect of the strength of the hydrophobic core in the sliding of CCs was also examined. Differences in the hydrophobic core and the electrostatic patterns between P and AP CCs may suggest that their sliding speeds are different.

Kinetic analysis of CC sliding

The effect of electrostatic interactions

To study sliding of homodimeric CCs, we used coarse-grained models in which the core interactions (between residues at the *a* and *d* positions) are of the same strength while allowing changes of registry. Accordingly, the interaction between residues at the *a* and *d* sites in a given heptad were symmetrized to allow change in registry while keeping the stability of the interface unchanged. A similar approach was implemented to predict the structure of the laminin CC protein (38). The effect that electrostatic interactions may have on the sliding dynamics of CCs was studied by designing several sequences that differ in their charges at the *e* and *g* positions. The pattern of charges was selected so that the number of salt bridges would change when sliding takes place. We concentrated on CCs with fewer salt bridges because we hypothesized that highly stable CC may prevent sliding. In this study, the *e* and *g* can be either positively or negatively charged. Where all the *e* and *g* charges are positive (or negative), the consequent repulsion strongly frustrates the CC structure (100% frustration). Where the charges are entirely complementary, the strong attraction between them reduces electrostatic frustration of binding to 0%, whereas a situation of 50% frustration occurs when attraction exists between half of the *e* and *g* pairs together with repulsion between the other *e* and *g* pair. Thus, a CC characterized before sliding by a maximal number of salt bridges between the *e* and *g* positions (two salt bridges per heptad and 0% electrostatic frustration) that lost all of its salt bridges after sliding one heptad (i.e., 100% electrostatic frustration) has moved from a state of 0% electrostatic frustration to a state of 100% electrostatic frustration, which is designated $P_{0\rightarrow 100}$ or $AP_{0\rightarrow 100}$, for P and AP CC, respectively.

Analysis of the first sliding event (i.e., a shift of one heptad) was performed by tracking the distance over time between the Cα beads of the *a* positions of the central heptad repeats of the two helices, as shown in Fig. 2. For the P conformation, the $P_{0\rightarrow 0}$ sequence showed the slowest rate (Fig. 2 *A*). Here, the wholly attractive electrostatic interactions between the *e* and *g* positions reduce frustration, which hinders sliding, and the system remains for a long time in its initial state. In general, after introducing structural frustration into the system by placing repulsive electrostatic interactions in the sequence, the dynamics increases and sliding becomes faster. In the $P_{0\rightarrow 100}$ model, electrostatic interactions are placed in such a way that before the one heptad repeat shift, all the *g*-*e* interactions are attractive, whereas after the one heptad repeat shift, they become wholly repulsive and the sliding time decreases in comparison to the ideal CC without electrostatic frustration (i.e., $P_{0\rightarrow 0}$). This occurs despite the presence of identical interactions within the hydrophobic core before and after the sliding in models $P_{0\rightarrow 0}$ and $P_{0\rightarrow 100}$. The $P_{50\rightarrow 50}$ model, which combines repulsive and attractive electrostatic interactions between the *e* and *g* positions, shows the fastest dynamics (Fig. 2 *B*). Thus, mutations in the *g*-*e* positions of the CC can modulate CC dynamics, and sliding is facilitated when both the initial and final states have some degree of electrostatic frustration.

Because our model system supports more than one sliding event, we constructed a color map that shows the probabilities of interface between the two helices after a registry shift. As shown in Fig. 2 *C*, the principal diagonal is more populated in the $P_{0\rightarrow 0}$ model compared to the other models, which have electrostatic frustration, in agreement with the observed first sliding times (Fig. 2 *B*). This indicates that this model remains in its initial conformation for longer times because of the attractive electrostatic interactions. Nevertheless, additional sliding events of one or two heptads in the direction of either the N- or the C-terminal can be observed by the populated four off-principal diagonals. In the same manner, the other two models exhibit different shifted conformations. However, the principal diagonal of the $P_{0\rightarrow 0}$ model, which lacks electrostatic frustration, is more populated than in the models that exhibit 50 or 100% electrostatic frustration of binding.

We then studied the effects of electrostatic interactions on the AP contribution. For this, we compared the time elapsed until the occurrence of the first one heptad sliding event in the purely electrostatically repulsive model, $AP_{100\rightarrow 100}$, to an intermediate electrostatically frustrated model, $AP_{50\rightarrow 50}$. As in the P case, the frustrated system, namely the $AP_{100\rightarrow 100}$, exhibits the faster dynamics (Fig. 2 *B*); however, the effects of the charges seem to be smaller than in the P conformation. Thus, although the dynamics can be modulated, repulsive interactions do not exert strong effects on the dynamics of AP CCs. It is worth noting here that the difference between the P and AP dynamics may also originate from the different way the hydrophobic core (i.e., interactions between the *a* and *d* positions) were modeled (see Methods for more details).

The effect of hydrophobic core residues

An evident parameter that can affect CC sliding dynamics is the strength of the hydrophobic core, which is created by the interactions between the residues in the *a* and *d* positions. To study this effect, we modulated the interaction strength of the hydrophobic core (ε) of the $P_{0\rightarrow 0}$ model. Fig. 3 shows that as ε decreases, the time elapsed until the first sliding

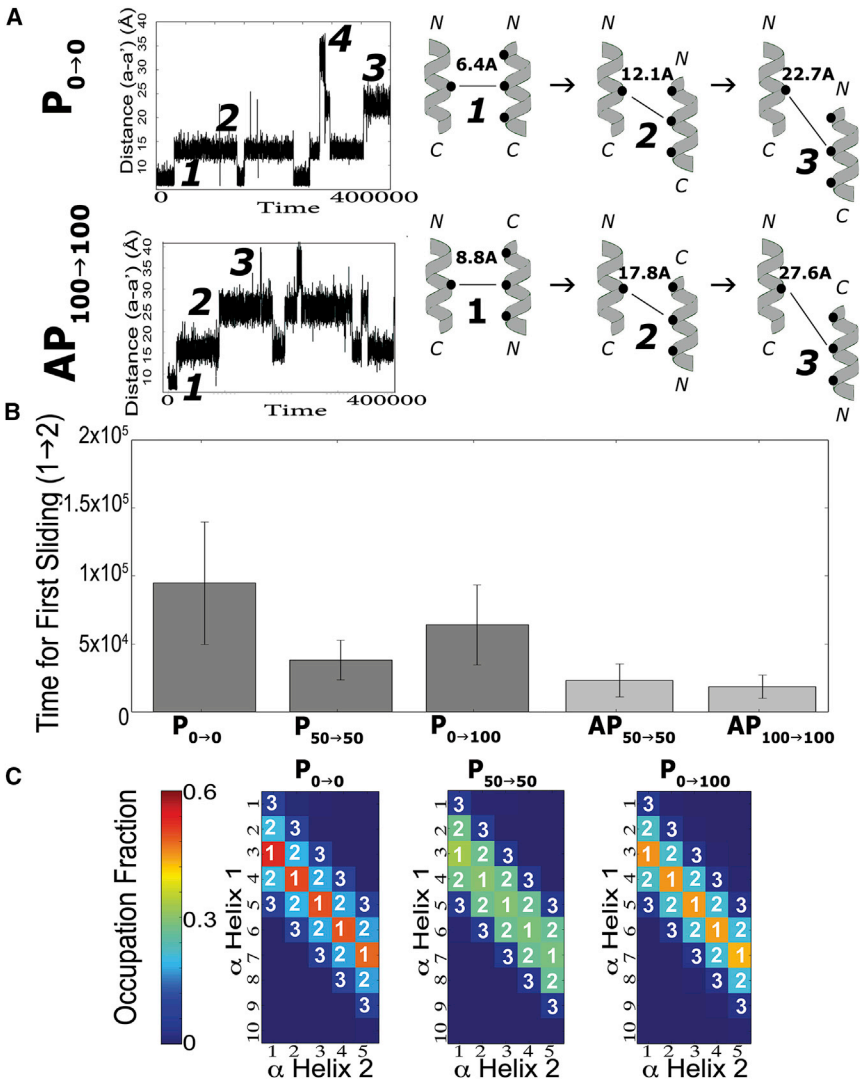

FIGURE 2 Kinetic analysis of CC sliding for P and AP configurations from coarse-grained MD simulations. (*A*) The time evolution of distances between the two neighboring helices in $P_{0\rightarrow0}$ and $AP_{100\rightarrow100}$ systems illustrating the change in registry due to sliding is shown. The subscripted numbers indicate the level of electrostatic frustration (0, 50, or 100% frustration modeled by the introduction of repulsive forces) between the *e* and *g* pairs before and after the first sliding event. The states, indicated by 1, 2, and 3, correspond to a shift of a single heptad or of two or three heptad repeats, respectively. The structures on the right illustrate the relative positions after sliding dynamics. (*B*) The kinetics of the first sliding event for five different CC sequences is shown. In general, electrostatic frustration at the beginning of the sliding process (such as exists in $P_{50\rightarrow50}$, $AP_{50\rightarrow50}$, and $AP_{50\rightarrow100}$) enhances CC sliding. The SD of the sliding kinetics is estimated from 50 simulations of each system. (*C*) Color maps of the total occupation fraction of the interface between the two helices of three CC systems are shown. The *x* and *y* axes correspond to different heptads of the short and long helices, respectively. The numbers correspond to the states indicated in (*A*). As electrostatic frustration increases, the population of the initial state (1) decreases. In the same manner, the population of secondary states (2,3) increases. To see this figure in color, go online.

of one heptad decreases. Thus, as the hydrophobic core becomes weaker, the CC exhibits faster sliding events. These results suggest that CCs increase their capability to sliding and become more dynamic either by increasing electrostatic frustration (by increasing repulsive forces) or by weakening the stability of the hydrophobic core (by decreasing hydrophobic interaction strength).

Energy landscape of CC sliding

To study the mechanism of sliding along a CC interface, we performed atomistic MD simulations using the umbrella sampling technique to plot the free energy along the reaction coordinate of the 1D sliding (see Methods). The potential of mean force along the sliding reaction coordinate was calculated for various sequences of P and AP homodimeric CCs with the aim of examining the effect of the residues at positions *a*, *d*, *e*, and *g* on the sliding mechanism. We ran umbrella sampling over 20 shifted structures that spanned a complete sliding event over one heptad repeat.

Fig. 4 *A* examines the effects that electrostatic interactions in the *g-e* positions and the strength of the hydrophobic core upon mutating the *a-d* positions exert on the energy landscape for sliding of P CC. To analyze the energy landscapes, five states were selected along the reaction coordinate (marked 1–5). The free-energy profile for sliding a single heptad at the interface of P CC is characterized by two energetic barriers, which are designated by states 2 and 4, respectively (the initial and final states of sliding are designated by states 1 and 5, respectively; Fig. 4 *A*). The electrostatic interactions between the *e* and *g* positions have a more pronounced effect on the height of the second barrier. Whereas the first barrier has a height of 1–1.5 kcal/mol, the height of the second barrier and the energy of the metastable state (states 4 and 3, respectively) between the two barriers are affected by electrostatic

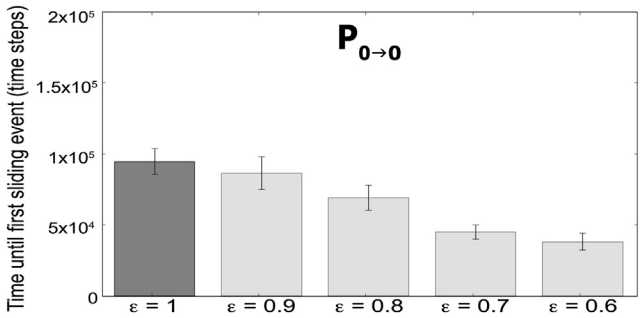

FIGURE 3 Sliding kinetics for the first heptad shift event. The sliding time is measured for the $P_{0\rightarrow 0}$ sequence (which has zero electrostatic frustration). Different hydrophobic core strengths were introduced by weakening the energetic contribution (ε) of contacts between residues in the *a* and *d* positions. Destabilization of the hydrophobic core enhances CC sliding kinetics. The SD of the sliding kinetics is estimated from 50 simulations of each system.

frustration. The propagation of sliding is facilitated in $P_{0\rightarrow 100}$ compared with $P_{0\rightarrow 0}$ because of electrostatic frustration. The existence of the electrostatic repulsions in the final state (state 5) is reflected by its higher free energy for systems $P_{0\rightarrow 100}$ than the corresponding state for system $P_{0\rightarrow 0}$. Accordingly, the sliding dynamics of the system $P_{0\rightarrow 100}$ is dominated by a single major barrier, whereas that of $P_{0\rightarrow 0}$ comprises two major barriers. For $P_{100\rightarrow 0}$, for which there is electrostatic frustration in the initial state, the energy landscape is more downhill than for the system $P_{0\rightarrow 100}$. Mutating the residues at position *a* from Asn to Leu ($P_{0\rightarrow 0}$ *(L-L)*) resulted in lowering the initial barrier for sliding, in agreement with previous studies that show the higher stability of the CC interface for Asn than Leu at positions *a* or *d* (24,41). Regardless of Asn or Leu at the *a* or *d* positions, the free-energy profile for sliding still has two major energetic barriers. Neutralization of the charges in the *e* and *g* positions (by mutating to Ser, $P_{No\ Charge}$ *(L-L)*) results in lowering the second barrier for sliding.

The energy landscape for sliding at the interface of AP CC differs from the corresponding landscape for P CC (Fig. 4 *B*). The energy landscape for sliding of AP CC is dominated by a single barrier that is relatively broad and located in the midtransition of the heptad sliding). The barrier height is ~1.5 kcal/mol, similarly to the two energetic barriers that govern sliding at P CC interfaces (located at the beginning and toward the end of the sliding event). We examined the effects of electrostatic frustration for the AP CC configurations and found it to be less pronounced than in the P CC (Fig. 4, *A* and *B*). When comparing the $AP_{100\rightarrow 100}$ CC with the $AP_{50\rightarrow 50}$, there is only a small reduction in the energy barrier, which agrees with the previously shown kinetic results in Fig. 2. Furthermore, deletion of charges in the *g-e* positions does not drastically change the energy profile of sliding at AP CC. Mutating the hydrophobic core of the $AP_{100\rightarrow 100}$ by introducing Leu residues in the *a* position instead of Ile hardly affects the free-energy profile for sliding.

Fig. 4 shows that the energy landscapes for a heptad shift for the P and AP CC configurations are different. In the P conformation, a metastable state can be observed after

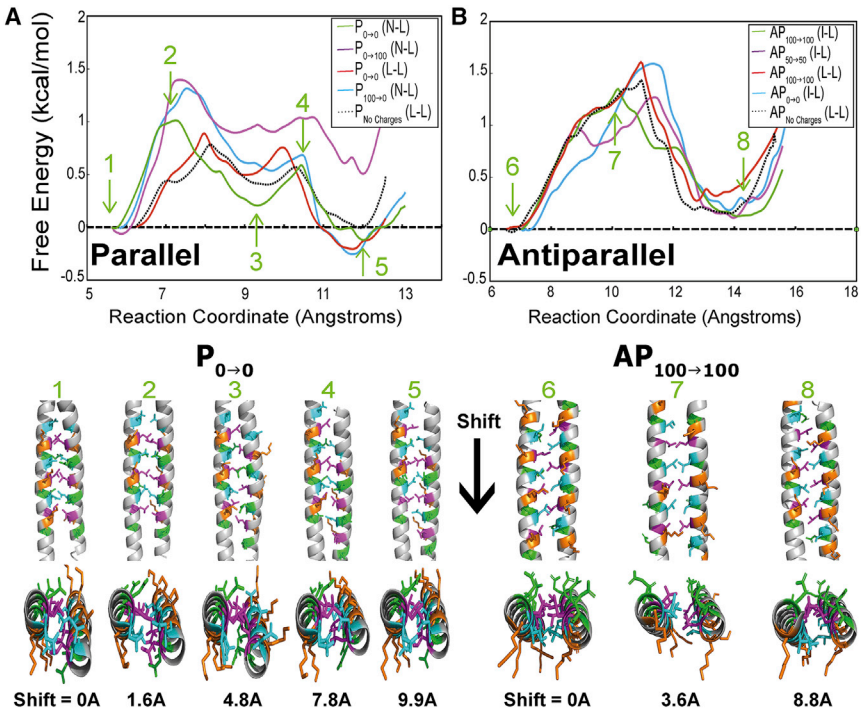

FIGURE 4 Energy landscape of sliding for P and AP CC configurations reconstructed by atomistic simulations. The energy landscape for sliding of a single heptad repeat was studied for several sequences of homodimeric CC using atomistic simulations while applying the umbrella sampling technique for enhanced sampling. The free-energy profile for CC sliding was studied for P CC (*A*) and AP CC (*B*) using the distance between two residues in *a* positions. The free-energy profiles for the P CC show three minima, whereas those for the AP exhibit only two main minima. The structural rearrangements that occur during sliding are illustrated by several snapshots taken from the unfrustrated $P_{0\rightarrow 0}$ system and from the maximally frustrated $AP_{100\text{-}100}$ CC system. The sequences of the studied CC are shown in Table S1. To see this figure in color, go online.

half of a heptad repeat unit slides. Here, the *a* positions of the hydrophobic core face the *d* positions. In this case, the hydrophobic core participates in different packing of the residues in the *a* and *d* positions, an arrangement that is less stable in the AP CC (states 3 and 7) comparing to the stable core of P CC. Shift in registry at the AP CC breaks the *a-d* interactions and exposes the residues at positions *a* and *d* to the solvent, as can be seen in the representative conformations in Fig. 4 *B*. After completion of one heptad sliding, the original hydrophobic packing recovers and the structure becomes stable again.

Bioinformatic analysis of CC sequences

To evaluate the prevalence of electrostatic frustration in the *g-e* positions, we performed a bioinformatics analysis of electrostatic frustration in sequences of natural homodimeric CCs that were collected using the server CC^{+} Database. We obtained a total of 390 homodimeric CCs of which 224 were P and 166 were AP homodimeric CCs. For every sequence, we calculated the number of attractive interactions in their crystal structure, following the rule for salt bridges of g_n:e_{n+1}' for P CC and e:e' or g:g' for AP CC.

In Fig. 5, we present a histogram of the percentage of attractive electrostatic interactions (i.e., salt bridges) for the 390 homodimeric CCs. The great majority of interactions between the *e* and *g* positions are not attractive for both P and AP configurations. Although the *e* and *g* positions are not saturated with charged residues (Fig. 5, *inset*), the origin of few salt bridges between these sites is also associated with imperfect pairing of the charges. P CCs present higher numbers of attractive interactions than that of the AP CCs, which suggests that some P CCs tend to be more stabilized by salt bridges than AP CCs. Thus, both P and AP CCs have high levels of frustration that may support shifted or staggered conformations in the α-helix pairing profile. Introducing electrostatic frustration was shown experimentally to reduce the thermodynamic stability of CC (42,43) and this in turn may facilitate sliding.

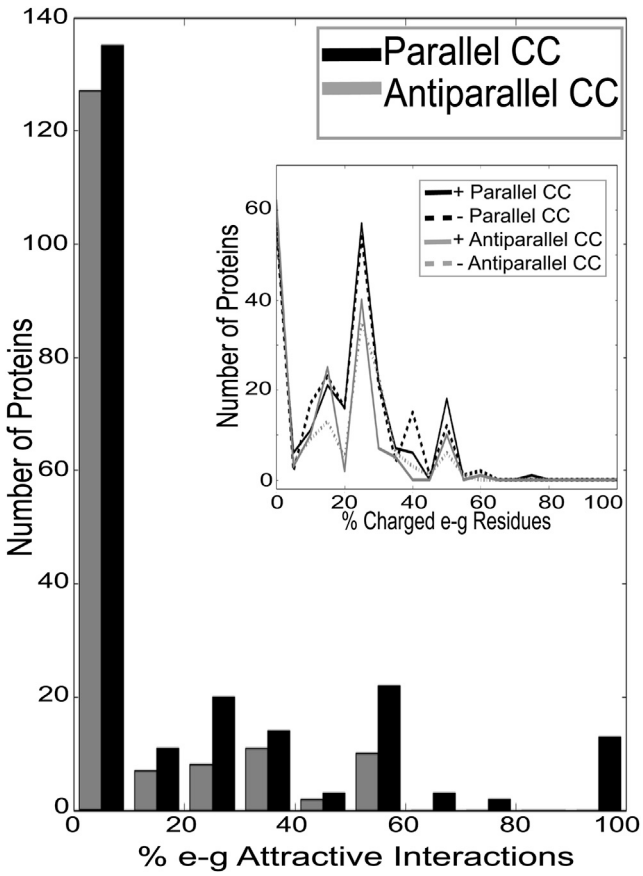

FIGURE 5 Bioinformatic analysis of attractive electrostatic interactions for homodimeric CC sequences. The analysis was performed on a data set of 390 proteins (obtained from the database provided by (54)) of which 224 were P and 166 were AP homodimeric CCs. P conformations exhibit a larger number of attractive electrostatic interactions (which corresponds to less frustration) than AP CCs. Thus, P CCs tend to be less dynamic and preserve the stable configuration more than the AP CCs. The inset highlights the total number of positive and negative charges at the *e* and *g* positions.

Experimental evidence for CC sliding

CC sliding in the nuclear pore

One example of sliding in natural CC systems is a shift of helices in the nucleoporin system. The nuclear pore complex is responsible for the selective exchange of macromolecules between the nucleus and cytoplasm in eukaryotic cells. The central channel of the nuclear pore complex is formed by several nucleoporin proteins (Nups): Nup62, Nup58, Nup54, and Nup45 (44). Nups are organized in a similar way in which N-terminal unstructured phenylalanine-glycine repeats are followed by ~200-residue α-helical CCs. The stable core of the Nup62 complex was identified, and the identical core domains of Nup58 and Nup45 were crystallized (45). The Nup58/45 protomer is an AP hairpin in which two α-helices (the N- and the C-helices) are connected by a short loop. The protomers dimerize in an AP way so that the helices of two protomers pack against each other by forming hydrophobic contacts at the CC interface (Fig. 6). The tetramer interface is formed by four N-helices of two dimers, which results in an AP orientation of the two dimers.

By superposition of pairs of the N-helices extracted from four different conformers in the crystal, four different configurational states can de distinguished. These states exhibit a lateral displacement (by up to ~11 Å) of the helices relative to each other and represent an alternative tetramerization interface. This interface is formed mostly by the hydrogen bonds between the side chains of six residues (Arg333, Gln344, Arg347, Gln348, Glu351, and Asn355) from each protomer. The lateral displacement results from alternative interactions between these residues (45).

To investigate the sliding mechanism between the CC interface of the Nup58/45 protomer, we performed MD

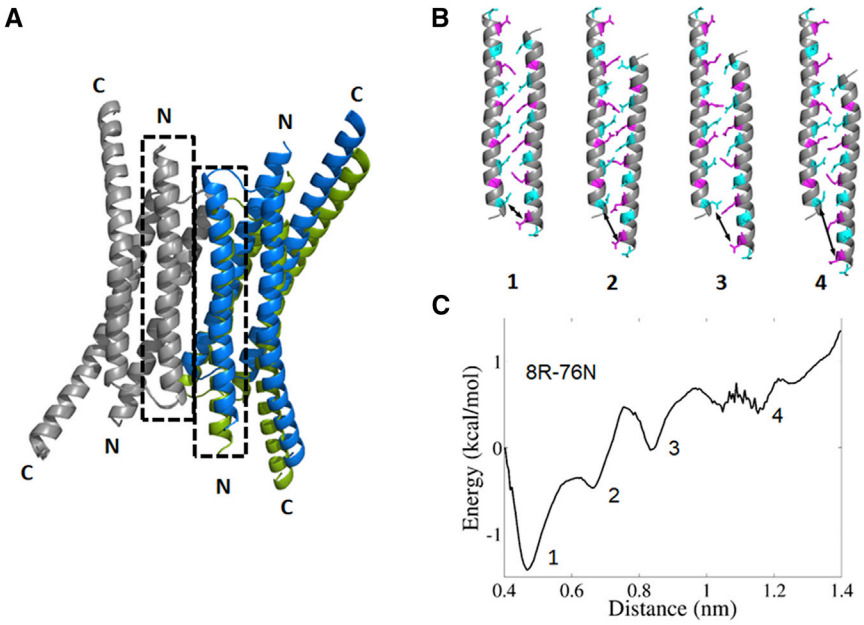

FIGURE 6 Sliding mechanism of the coiled-coil (CC) interface of Nup58/45. (*A*) The structure of the Nup58/45 (Protein Data Bank [PDB]: 2OSZ) illustrating a sliding dynamics of 11 Å along the CC interface of the N-helix is shown. (*B* and *C*) Potential of mean force for sliding dynamics along two isolated N-helices that form AP CC (marked by *dashed rectangles*) from atomistic MD simulations is shown. Four representative conformations, which are designated one to four and correspond to the four minima in the energy profile, illustrate the dynamics. In the structures, residues at *a* and *d* positions are colored in cyan and magenta, respectively. To see this figure in color, go online.

simulations using the umbrella sampling technique (see Methods). We simulated the four different conformers found for the Nup58/45 tetramer by studying the potential of mean force of the interactions between two interacting N-helices from two dimers within the tetramer (Fig. 6). Based on the free-energy profile along the sliding axis (Fig. 6), the transition between the four states captured experimentally involves energetic barriers, each of ~1 kcal/mol. These barriers are relatively low and support sliding in the Nup58/45 system, as was concluded from the x-ray structures. The existence of intermediate states in the sliding of AP CC might be due to its stabilization by other regions of the interface of the tetramer. Alternatively, the intermediate states may arise from the less hydrophobic character of the interface than is common for CC interfaces. We note that in contrast to the free-energy profiles shown in Fig. 6, the final state of the CC of Nup58/45 after sliding is less stable than the initial state simply because the interface became smaller by one heptad. In the sliding of all the CC systems shown in Fig. 4, the size of the interface was held constant during sliding dynamics.

CC sliding in dynein stalk region

A prominent example of a CC is the dynein stalk region, an AP CC that has the capacity to transmit structural changes in the ATPase domain toward the MTBD. The existence of two discrete registries in the CC domain has been experimentally determined. One is known as the $+\beta$ registry or the low-affinity microtubule-binding structure, and the second one is the α registry or the high-affinity microtubule-binding mode (see Fig. 7). Despite the large number of studies, how the change in registry takes place in the AP CC is not entirely clear, and different models have been proposed (17,36,46,47).

The most accepted mechanism for the conformational change of the dynein CC is the sliding model (17,31,47) that starts with the dynein being in the $+\beta$ registry. After hydrolysis of ATP, the first helix of the stalk CC (CC1) slides by a half heptad repeat with respect to the second helix of the stalk CC (Fig. 7, model 1). This sliding motion is supported by the secondary CC buttress. Thus, the hydrophobic residues in the *d* position of CC1 shift toward the previously occupied *a* positions (46). This unpacks the hydrophobic core and exposes the *a-d* residues to solvent, as shown in structure 7 of Fig. 4. This model is supported by a large number of structural and biochemical studies (17,36,46,47). Moreover, half heptad sliding transitions have also been observed in other CCs (32,48).

A sliding mechanism can explain experimental observations; however, it does not constitute direct proof that CC sliding actually takes place. It was argued that the sliding mechanism might be too costly energetically and thus unfavorable. An alternative mechanism, therefore, was proposed for CC stalk registry change (46). Following this mechanism, a structural change in the buttress CC is coupled to Pi release from the AAA+ ring. This immediately leads to a structural change at the beginning of the stalk domain that is carried over the whole CC like a zipper. In this way, the AP CC changes its registry from β to α, (Fig. 7, model 2). Another alternative and more extreme mechanism was proposed, suggesting that the change in registry takes place only after the stalk domain unfolds (47) (Fig. 7, model 3). Strong evidence against this mechanism is the experimental observation that the stalk domain does not show large structural changes during the dynein motor cycle (47,49,50).

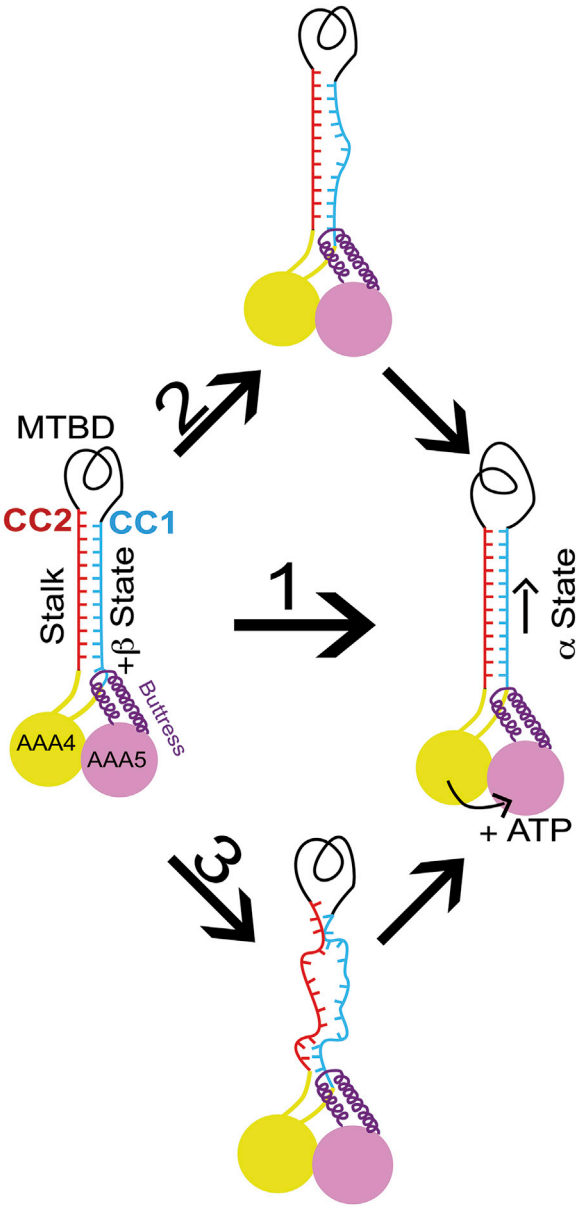

FIGURE 7 Proposed models for the change of registry in the stalk AP CC of the dynein microtubule-binding domain (MTBD). In the most accepted model 1, the first coiled-coil helix (CC1) slides a half heptad repeat with respect to the second helix of the stalk CC, so losing its hydrophobic packaging and becoming exposed to the solvent (17,47). This model is supported by a large number of structural and biochemical studies (17,36,46,47). An alternative proposed model 2 suggests that a conformational change at the beginning of the CC is carried over along the whole CC, following a zipper model (46). The third and least accepted model for the change of registry in the dynein CC stalk domain is the one in which a melting of the CC is followed by a change in the registry of the CC (model 3) (47). To see this figure in color, go online.

Although no consensus exists concerning the mechanisms governing the change of registry of the stalk domain, this computational study suggests that sliding at the CC interface is likely. Although sliding of AP CCs demands crossing a barrier of ~1.5 kcal/mol, as can be observed in the energy landscape shown in Fig. 4 *B*, ATP hydrolysis can provide enough energy to overcome the energy barrier. Because a typical hydrolysis event releases energy of ~7 kcal/mol, the dynein motor cycle would be provided with enough energy to overcome the energy barrier. Moreover, it is noteworthy that dynein has hydrophobic residues only in the *d* positions and not in the *a* positions; thus, the energetic barrier for sliding might be lower and therefore more favorable. The sliding mechanism for dynein is also supported by several experimental structures that show a shift of a full heptad and not by a half heptad, which we find to be especially unstable for AP CC.

Sliding for P CC

Sliding dynamics was also probed experimentally for P CC. Single-molecule experiments that were undertaken for two stable P CCs (a variant of the leucine zipper GCN4 and a heterodimer pER) suggested that helix sliding is a general feature of CCs because of their periodic structure (30). Staggered CC conformations were probed for these two systems, which differ in their sequence, stability, and orientation. Furthermore, the single-molecule study supports the existence of staggered intermediate CC structures (36), consistent with the intermediate state (with sliding of half a heptad) found in the free-energy landscape for sliding of P CC (Fig. 4).

CONCLUSIONS

In this study, sliding at the interface of homodimeric CCs was explored using coarse-grained and atomistic MD simulations. The coarse-grained models were used to obtain kinetic information about the sliding of P and AP conformations with different sequences, particularly the identity of the residues at position *a* and *d* as well as *e* and *g*. Charges at positions *e* and *g*, which form salt bridges with the neighboring helical peptide, may stabilize the CC and will disfavor sliding dynamics. Repulsive electrostatic interactions between residues in these positions constitute electrostatic frustration within the CC structure that may facilitate sliding dynamics. The important role of electrostatic interactions in promoting 1D diffusion at the CC interface is reminiscent to the effect of long-range electrostatic interactions in the sliding of proteins along dsDNA (3). In addition to the role of electrostatic frustration, decreasing the stability of the interface by reducing the strength of the interactions between *a* and *d* at the hydrophobic core of the CC results in faster diffusion. A similar trade-off between stability and speed was also reported for the sliding of proteins along dsDNA (51).

The energy landscapes for registry shifts suggest a different mechanism for sliding along P and AP CCs. Sliding of P CC conformations takes place via a metastable state in which half a heptad repeat is shifted, whereas sliding of AP CC configuration is achieved via

a higher and wider energetic barrier. The energy landscape for sliding is affected by sequence variations, with the sliding of P CC being more sensitive to mutations than the AP CC. Introducing electrostatic frustration reduces the barrier for sliding more significantly in the P than the AP CC, consistent with the results from the coarse-grained simulations. Nevertheless, electrostatic and hydrophobic frustration facilitate the sliding of CCs in both configurations. Our results suggest that the proposed sliding mechanism for the stalk CC in the dynein protein can take place after an ATP molecule is hydrolyzed in the head of the protein and a structural change takes place in the protein. This provides insights into the role of CCs in signaling transduction.

Sliding at CC interfaces, although it was shown for several systems, is less characterized than for protein sliding along nucleic acids. Our results indicate that sliding is an intrinsic property of these systems and may exhibit similar features in all of them; however, they may depend on the sequence of the CC. In comparison to sliding along dsDNA, the energetic barriers to sliding along CC are higher, being ~1–1.5 kcal/mol, whereas those for sliding along dsDNA are 0.6–1.2 kcal/mol. Sliding along the CC interface is therefore expected to be less widespread and of limited length scale. Nevertheless, sliding can be a mechanism for conformational changes or allosteric communication along CCs that require concerted changes in the CC registry and helix packing with a global change of ~10 Å in CCs, which correspond to sliding of one heptad repeat. Further quantifications are required to address sliding in CCs of higher oligomeric states and of a heteroligomeric nature as well as the possibility that CC sliding involves unwinding of the helices (52,53). It is likely that sliding dynamics is more widespread in molecular biology than originally considered and is relevant to other biomolecular systems in which sliding at protein-protein interfaces potentially plays a role in functional dynamics.

SUPPORTING MATERIAL

Supporting Material can be found online at https://doi.org/10.1016/j.bpj.2019.02.026.

AUTHOR CONTRIBUTIONS

D.G., Y.G., and Y.L. conceived the study and designed the research. D.G. and Y.G. performed the research and analyzed data. D.G., Y.G., and Y.L. wrote the manuscript.

ACKNOWLEDGMENTS

This work was supported by the Israel Science Foundation and by the Minerva Foundation, with funding from the Federal German Ministry for Education and Research. Y.L. is the Morton and Gladys Pickman Professional Chair in Structural Biology.

SUPPORTING CITATIONS

Reference (54) appears in the Supporting Material.

REFERENCES

1. Marklund, E. G., A. Mahmutovic, …, J. Elf. 2013. Transcription-factor binding and sliding on DNA studied using micro- and macroscopic models. *Proc. Natl. Acad. Sci. USA.* 110:19796–19801.
2. Blainey, P. C., G. Luo, …, X. S. Xie. 2009. Nonspecifically bound proteins spin while diffusing along DNA. *Nat. Struct. Mol. Biol.* 16:1224–1229.
3. Givaty, O., and Y. Levy. 2009. Protein sliding along DNA: dynamics and structural characterization. *J. Mol. Biol.* 385:1087–1097.
4. Mishra, G., and Y. Levy. 2015. Molecular determinants of the interactions between proteins and ssDNA. *Proc. Natl. Acad. Sci. USA.* 112:5033–5038.
5. Roy, R., A. G. Kozlov, …, T. Ha. 2009. SSB protein diffusion on single-stranded DNA stimulates RecA filament formation. *Nature.* 461:1092–1097.
6. Hinrichs, M. H., A. Jalal, …, T. Scholz. 2012. Tau protein diffuses along the microtubule lattice. *J. Biol. Chem.* 287:38559–38568.
7. Cooper, J. R., and L. Wordeman. 2009. The diffusive interaction of microtubule binding proteins. *Curr. Opin. Cell Biol.* 21:68–73.
8. Kamagata, K., E. Mano, …, R. C. Johnson. 2018. High free-energy barrier of 1D diffusion along DNA by architectural DNA-binding proteins. *J. Mol. Biol.* 430:655–667.
9. Tan, C., T. Terakawa, and S. Takada. 2016. Dynamic coupling among protein binding, sliding, and DNA bending revealed by molecular dynamics. *J. Am. Chem. Soc.* 138:8512–8522.
10. Potoyan, D. A., C. Bueno, …, P. G. Wolynes. 2017. Resolving the NFκB heterodimer binding paradox: strain and frustration guide the binding of dimeric transcription factors. *J. Am. Chem. Soc.* 139:18558–18566.
11. Khazanov, N., and Y. Levy. 2011. Sliding of p53 along DNA can be modulated by its oligomeric state and by cross-talks between its constituent domains. *J. Mol. Biol.* 408:335–355.
12. Marcovitz, A., and Y. Levy. 2011. Frustration in protein-DNA binding influences conformational switching and target search kinetics. *Proc. Natl. Acad. Sci. USA.* 108:17957–17962.
13. Truebestein, L., and T. A. Leonard. 2016. Coiled-coils: the long and short of it. *BioEssays.* 38:903–916.
14. Walshaw, J., and D. N. Woolfson. 2001. Socket: a program for identifying and analysing coiled-coil motifs within protein structures. *J. Mol. Biol.* 307:1427–1450.
15. Burkhard, P., J. Stetefeld, and S. V. Strelkov. 2001. Coiled coils: a highly versatile protein folding motif. *Trends Cell Biol.* 11:82–88.
16. Südhof, T. C., and J. E. Rothman. 2009. Membrane fusion: grappling with SNARE and SM proteins. *Science.* 323:474–477.
17. Carter, A. P., C. Cho, …, R. D. Vale. 2011. Crystal structure of the dynein motor domain. *Science.* 331:1159–1165.
18. del Rio, A., R. Perez-Jimenez, …, M. P. Sheetz. 2009. Stretching single talin rod molecules activates vinculin binding. *Science.* 323:638–641.
19. Mason, J. M., and K. M. Arndt. 2004. Coiled coil domains: stability, specificity, and biological implications. *ChemBioChem.* 5:170–176.
20. Lupas, A. N., and J. Bassler. 2017. Coiled coils - a model system for the 21st century. *Trends Biochem. Sci.* 42:130–140.
21. Moutevelis, E., and D. N. Woolfson. 2009. A periodic table of coiled-coil protein structures. *J. Mol. Biol.* 385:726–732.
22. Fletcher, J. M., R. L. Harniman, …, D. N. Woolfson. 2013. Self-assembling cages from coiled-coil peptide modules. *Science.* 340:595–599.
23. Huang, P. S., G. Oberdorfer, …, D. Baker. 2014. High thermodynamic stability of parametrically designed helical bundles. *Science.* 346:481–485.

24. Woolfson, D. N. 2005. The design of coiled-coil structures and assemblies. *Adv. Protein Chem.* 70:79–112.

25. Piñeiro, A., A. Villa, …, A. E. Mark. 2005. A molecular dynamics study of the formation, stability, and oligomerization state of two designed coiled coils: possibilities and limitations. *Biophys. J.* 89:3701–3713.

26. Hadley, E. B., O. D. Testa, …, S. H. Gellman. 2008. Preferred side-chain constellations at antiparallel coiled-coil interfaces. *Proc. Natl. Acad. Sci. USA.* 105:530–535.

27. Schug, A., P. C. Whitford, …, J. N. Onuchic. 2007. Mutations as trapdoors to two competing native conformations of the Rop-dimer. *Proc. Natl. Acad. Sci. USA.* 104:17674–17679.

28. Levy, Y., S. S. Cho, …, P. G. Wolynes. 2005. Symmetry and frustration in protein energy landscapes: a near degeneracy resolves the Rop dimer-folding mystery. *Proc. Natl. Acad. Sci. USA.* 102:2373–2378.

29. Gambin, Y., A. Schug, …, A. A. Deniz. 2009. Direct single-molecule observation of a protein living in two opposed native structures. *Proc. Natl. Acad. Sci. USA.* 106:10153–10158.

30. Xi, Z., Y. Gao, …, Y. Zhang. 2012. Single-molecule observation of helix staggering, sliding, and coiled coil misfolding. *Proc. Natl. Acad. Sci. USA.* 109:5711–5716.

31. Kon, T., K. Imamula, …, K. Sutoh. 2009. Helix sliding in the stalk coiled coil of dynein couples ATPase and microtubule binding. *Nat. Struct. Mol. Biol.* 16:325–333.

32. Croasdale, R., F. J. Ivins, …, M. Pfuhl. 2011. An undecided coiled coil: the leucine zipper of Nek2 kinase exhibits atypical conformational exchange dynamics. *J. Biol. Chem.* 286:27537–27547.

33. Snoberger, A., E. J. Brettrager, and D. M. Smith. 2018. Conformational switching in the coiled-coil domains of a proteasomal ATPase regulates substrate processing. *Nat. Commun.* 9:2374.

34. Stewart, C. M., C. Z. Buffalo, …, P. Ghosh. 2016. Coiled-coil destabilizing residues in the group A Streptococcus M1 protein are required for functional interaction. *Proc. Natl. Acad. Sci. USA.* 113:9515–9520.

35. O'Shea, E. K., J. D. Klemm, …, T. Alber. 1991. X-ray structure of the GCN4 leucine zipper, a two-stranded, parallel coiled coil. *Science.* 254:539–544.

36. Schmidt, H., R. Zalyte, …, A. P. Carter. 2015. Structure of human cytoplasmic dynein-2 primed for its power stroke. *Nature.* 518:435–438.

37. Ferreiro, D. U., E. A. Komives, and P. G. Wolynes. 2014. Frustration in biomolecules. *Q. Rev. Biophys.* 47:285–363.

38. Armony, G., E. Jacob, …, D. Fass. 2016. Cross-linking reveals laminin coiled-coil architecture. *Proc. Natl. Acad. Sci. USA.* 113:13384–13389.

39. Azia, A., and Y. Levy. 2009. Nonnative electrostatic interactions can modulate protein folding: molecular dynamics with a grain of salt. *J. Mol. Biol.* 393:527–542.

40. Wood, C. W., M. Bruning, …, D. N. Woolfson. 2014. CCBuilder: an interactive web-based tool for building, designing and assessing coiled-coil protein assemblies. *Bioinformatics.* 30:3029–3035.

41. Woolfson, D. N., and T. Alber. 1995. Predicting oligomerization states of coiled coils. *Protein Sci.* 4:1596–1607.

42. Monera, O. D., N. E. Zhou, …, R. S. Hodges. 1993. Comparison of antiparallel and parallel two-stranded alpha-helical coiled-coils. Design, synthesis, and characterization. *J. Biol. Chem.* 268:19218–19227.

43. Monera, O. D., C. M. Kay, and R. S. Hodges. 1994. Electrostatic interactions control the parallel and antiparallel orientation of alpha-helical chains in two-stranded alpha-helical coiled-coils. *Biochemistry.* 33:3862–3871.

44. Guan, T., S. Müller, …, L. Gerace. 1995. Structural analysis of the p62 complex, an assembly of O-linked glycoproteins that localizes near the central gated channel of the nuclear pore complex. *Mol. Biol. Cell.* 6:1591–1603.

45. Melcák, I., A. Hoelz, and G. Blobel. 2007. Structure of Nup58/45 suggests flexible nuclear pore diameter by intermolecular sliding. *Science.* 315:1729–1732.

46. Nishikawa, Y., M. Inatomi, …, G. Kurisu. 2016. Structural change in the dynein stalk region associated with two different affinities for the microtubule. *J. Mol. Biol.* 428 (9 Pt B):1886–1896.

47. Carter, A. P., and R. D. Vale. 2010. Communication between the AAA+ ring and microtubule-binding domain of dynein. *Biochem. Cell Biol.* 88:15–21.

48. Macheboeuf, P., C. Buffalo, …, P. Ghosh. 2011. Streptococcal M1 protein constructs a pathological host fibrinogen network. *Nature.* 472:64–68.

49. Roberts, A. J., N. Numata, …, S. A. Burgess. 2009. AAA+ ring and linker swing mechanism in the dynein motor. *Cell.* 136:485–495.

50. Ueno, H., T. Yasunaga, …, K. Hirose. 2008. Dynein pulls microtubules without rotating its stalk. *Proc. Natl. Acad. Sci. USA.* 105:19702–19707.

51. Zandarashvili, L., A. Esadze, …, J. Iwahara. 2015. Balancing between affinity and speed in target DNA search by zinc-finger proteins via modulation of dynamic conformational ensemble. *Proc. Natl. Acad. Sci. USA.* 112:E5142–E5149.

52. Goktas, M., C. Luo, …, K. G. Blank. 2018. Molecular mechanics of coiled coils loaded in the shear geometry. *Chem. Sci. (Camb.).* 9:4610–4621.

53. Luo, C., K. G. Blank, …, A. V. Verde. 2017. Mechanism of coiled-coil deformation under tension strongly depends on the pull speed. *Eur Biophys J Biophy.* 46:S222.

54. Testa, O. D., E. Moutevelis, and D. N. Woolfson. 2009. CC+: a relational database of coiled-coil structures. *Nucleic Acids Res.* 37:D315–D322.